Chemical and Electronic Structure at the Interface between a Sputter-Deposited Zn(O,S) Buffer and a Cu(In,Ga)(S,Se)$_2$ Solar Cell Absorber

Dirk Hauschild,* Mary Blankenship, Amandee Hua, Ralph Steininger, Patrick Eraerds, Thomas Niesen, Thomas Dalibor, Wanli Yang, Clemens Heske, and Lothar Weinhardt

The chemical and electronic structure of the interface between a sputter-deposited Zn(O,S) buffer layer and an industrial Cu(In,Ga)(S,Se)$_2$ (CIGSSe) absorber for thin-film solar cells is investigated with X-ray and UV photoelectron spectroscopy, inverse photoemission spectroscopy, and X-ray emission spectroscopy. We find a CIGSSe absorber surface band gap of 1.61 ($\pm$0.14) eV, which is significantly increased as compared to the minimal value derived with bulk-sensitive methods ($\approx$1.1 eV). We find no indication for diffusion of absorber elements into the buffer layer. Surface- and bulk-sensitive measurements of the buffer layer suggest the presence of S-Zn and S-O bonds in the Zn(O,S) layer. We find that the naturally existing downward band bending toward the CIGSSe absorber surface is increased by the formation of the interface, likely enhancing carrier separation under illumination. We also derive a flat conduction band alignment, in line with the reported high conversion efficiencies of corresponding large-area solar cells.

1. Introduction

The efficiency of Cu(In,Ga)(S,Se)$_2$-based (CIGSSe) thin-film solar cells has increased significantly over the last few years, both on the laboratory and module scale. Such high efficiencies are commonly achieved with a CdS buffer layer deposited via chemical bath deposition (CBD). For a commercial product, however, a Cd-free buffer layer compatible with an in-line production is

desirable. Very promising results have been achieved with indium sulfide-based buffer layers, reaching a record efficiency of up to 17.9% on 30 × 30 cm^2.[1] One issue with this buffer is the diffusion of copper from the absorber into the buffer layer during further process steps, which reduces the buffer layer band gap and increases its light absorption.[2–4] This effect was partially mitigated by incorporating sodium into the buffer layer.[5] Another promising buffer layer material is Zn(O,S), for which the band gap can be varied from 2.6 to 3.4 eV by changing the O/S ratio.[6] In fact, Solar Frontier has achieved (lab-scale) efficiencies as high as 23.35% with a Zn(O,S, OH)$_x$-based buffer layer.[7]

To further enhance the efficiency of CIGSSe-based solar cells with a particular choice of buffer material, the absorber also needs to be adapted. Among others, the absorber's Ga/(Ga+In) (GGI) and S/(S + Se) (SSSe) ratio and its profile (i.e., depth variation) can be optimized,[8] and the resulting surface properties of the absorber will play an important role when the interface to the buffer layer is formed. Such an optimization needs to be supported by a detailed characterization of the materials and their surfaces. In particular, the chemical and electronic properties at the buffer/absorber interface are crucial for solar cell efficiency

D. Hauschild, C. Heske, L. Weinhardt
Institute for Chemical Technology and Polymer Chemistry (ITCP)
Karlsruhe Institute of Technology (KIT)
Engesserstr. 18/20, 76128 Karlsruhe, Germany
E-mail: dirk.hauschild@kit.edu

D. Hauschild, R. Steininger, C. Heske, L. Weinhardt
Institute for Photon Science and Synchrotron Radiation (IPS)
Karlsruhe Institute of Technology (KIT)
Hermann-v.-Helmholtz-Platz 1, 76344 Eggenstein-Leopoldshafen, Germany

The ORCID identification number(s) for the author(s) of this article can be found under https://doi.org/10.1002/solr.202201091.

D. Hauschild, M. Blankenship, A. Hua, C. Heske, L. Weinhardt
Department of Chemistry and Biochemistry
University of Nevada, Las Vegas (UNLV)
4505 Maryland Parkway, Las Vegas, NV 89154-4003, USA

P. Eraerds, T. Niesen, T. Dalibor
AVANCIS GmbH
Otto-Hahn-Ring 6, 81739 Munich, Germany

W. Yang
Advanced Light Source
Lawrence Berkeley National Laboratory
1 Cyclotron Road, Berkeley, CA 94720, USA

and thus need to be monitored. This includes information about the buffer layer growth, interdiffusion, and the band alignment at the buffer/absorber interface.

Previous studies on CBD Zn(O,S) buffer layers with Cu(In,Ga)Se$_2$ (CIGSe) absorbers from the National Renewable Energy Laboratory (NREL) revealed a flat conduction band alignment at the buffer/absorber interface, an intermixing of Se into the buffer, as well as Zn in various bonding environments, e.g., ZnS, ZnO, ZnSe, and Zn(OH)$_2$.[9–11] For other Zn(O,S)/CIGSe samples, a high defect concentration, inducing Fermi level pinning, was reported.[12] Studies of CuInS$_2$ (CIS) absorbers show the formation of a Zn(O,S)/ZnS bilayer at the CBD-Zn(O,S)/CIS interface[13] and a small spike in the conduction band alignment.[14] Recently, it was proposed that near-interface defects might be present in devices with poor performance.[15]

Previously, CIGSSe absorbers made by AVANCIS GmbH contained a composition gradient of sulfur and selenium but showed only trace amounts of Ga at the surface.[5,16–19] For the present study, the gallium gradient was modified, such that Ga is now also present at the surface in quantities easily detectable by photoelectron spectroscopy. This, in turn, is expected to increase the band gap at the surface.[20] Using the sputter-deposited Zn(O,S) buffer layer, which makes the intrinsic (i.e., not actively doped) ZnO layer obsolete,[21] module efficiencies up to 18.1% can be reached. With a postdeposition treatment (PDT), this efficiency is increased to 19.8%.[22]

To comprehensively describe the chemical and electronic structure at this novel high-efficiency Ga-containing Zn(O,S)/Cu(In,Ga)(S,Se)$_2$ interface, a combination of X-ray photoelectron spectroscopy (XPS), X-ray excited Auger electron spectroscopy (XAES), synchrotron-based soft X-ray emission spectroscopy (XES), ultraviolet photoelectron spectroscopy (UPS), and inverse photoemission spectroscopy (IPES) was employed.

2. Results

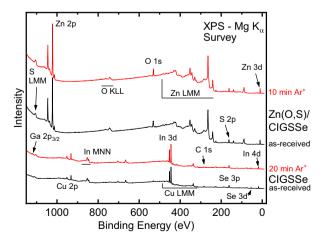In **Figure 1**, the XPS (Mg K_α excitation) survey spectra of the CIGSSe absorber and the fully buffered Zn(O,S)/CIGSSe sample are presented. In the survey spectra of the as-received CIGSSe absorber (black), all signals of the absorber elements (e.g., Ga 2p, Cu 2p, In 3d, S 2p, and Se 3d) are visible. The Ga 2p peak intensity is small, suggesting only a small gallium content at the surface, as will be analyzed in detail below. In addition, small O and C 1s peaks are detected, which decrease (most notably the C 1s peak) after a 20 min 50 eV low-energy Ar$^+$ surface treatment. This suggests the presence of C- and O-containing surface adsorbates.

For the thickest Zn(O,S) buffer layer on CIGSSe, Zn-, O-, and S-related lines are visible, while no absorber-related lines can be detected. This indicates that the Zn(O,S) buffer layer forms a closed layer and that no (strong) diffusion of absorber elements into the Zn(O,S) occurs (as we will discuss in the following). After a 10 min Ar$^+$-ion treatment, almost no change in the survey spectrum is visible, suggesting that the as-received sample features only very little amounts of surface adsorbates. Note that the O 1s core level consists of two components, barely visible on the scale of Figure 1. A detailed binding energy analysis (see Figure S1, Supporting Information) identifies the components as an "oxide-like" and a "hydroxide-like" species[23,24] and will be discussed later.

Traditionally, the Avancis SEL-RTP-produced absorbers only show trace amounts of Ga at the surface, as pointed out in our earlier publications.[5,16–19] In the modified process, with altered Ga distribution for optimal matching with the Zn(O,S) buffer (as we will show throughout this paper), Ga is now also easily found at the surface, as seen by the Ga 2p line in the absorber survey spectrum (Figure 1) and the Ga 3d contributions in the Ga 3d/In 4d region in **Figure 2**. To analyze the chemical environment of Ga and In at the surface, we performed a fit analysis of the In 4d/Ga 3d region with a linear background and two sets of Voigt profiles (the Lorentzian and Gaussian widths for the two In 4d and Ga 3d components were kept identical, respectively), fixing the peak area ratio according to the 2j + 1 multiplicity (note that, strictly speaking, this region of shallow core levels should be described in a dispersive band-structure model, the complexity of which is beyond the simple stoichiometry
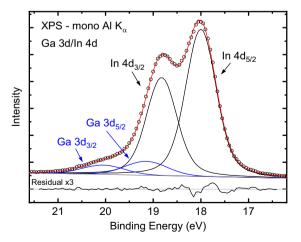

Figure 1. XPS survey spectra excited with Mg K_α of the as-received (black) and Ar$^+$-ion-treated (red) CIGSSe absorber and the fully buffered Zn(O,S)/CIGSSe sample. Prominent photoemission and Auger features are labeled.

Figure 2. Ga 3d/In 4d spectral region (excited with monochromatized Al K_α) of the CIGSSe absorber (open circles). The fit (red) highlights the Ga 3d (blue) and In 4d (black) spectral contributions. The magnified residual (x3) is shown below the spectrum.

quantification attempted here). The spin-orbit splitting, in contrast, was not constrained. The binding energy of the Ga $3d_{5/2}$ is 19.18 (± 0.02) eV, which is close to the position of 19.08 eV found for an S-free CIGSe surface of a three-stage processed absorber (with a GGI of ≈ 0.30).[25,26] This suggests that gallium is in a chalcopyrite environment (as expected), which is further supported by the modified Ga Auger parameter α'_{Ga} (i.e., the sum of the binding energy of the Ga $2p$ line and the kinetic energy of the Ga $L_3M_{4,5}M_{4,5}$ signal). It is found to be 2183.23 (± 0.15) eV, in agreement with chalcopyrite literature values.[23,27,28] Similarly, the In $4d_{5/2}$ peak is found at 18.00 eV and the modified In Auger parameter α'_{In}, determined using the In $3d_{5/2}$ binding energy and In $M_4N_{4,5}N_{4,5}$ kinetic energy, was found to be 852.54 (± 0.15) eV. This value is in good agreement with the Ga-free Avancis CuIn(S,Se)$_2$ absorber surface ($\alpha'_{In} = 852.58$ eV)[5] and other chalcopyrite absorbers.[23,27,29]

To analyze the Zn(O,S)/CIGSSe interface formation, the prominent absorber-related lines are shown in **Figure 3** as a function of increasing buffer layer thickness of the as-received sample set. As expected, the Ga $2p$, Cu $2p$, In $3d$, and Se $3d$ lines decrease in intensity with increasing Zn(O,S) buffer layer thickness. The low kinetic-energy signals (Ga and Cu $2p$) are governed by a smaller characteristic inelastic mean free path (IMFP) λ ($\lambda_{Ga\ 2p} \approx 0.6$ nm), while the other lines feature faster electrons and are hence less surface-sensitive (e.g., $\lambda_{Se\ 3d} \approx 2.5$ nm).[30,31] Note that the IMFP neglects elastic-scattering effects—using the effective attenuation length (EAL), which accounts for elastic scattering[32]—we obtain a $\approx 20\%$ larger characteristic attenuation length in our measurement geometry.[33] For the 10 nm Zn(O,S)/CIGSSe sample, only the strongest peaks (In and Se $3d$) are still detected, while, for the thickest buffer layer, no absorber-related peaks can be observed. This suggests that the Zn(O,S) buffer layer is completely closed and that no (long-range) diffusion of absorber elements occurs.

In addition to the intensity decrease with increasing Zn(O,S) buffer layer thickness, peak shifts are detected, which will be analyzed later in this paper. On the absorber surface, a small Na signal is detected as well (Figure S2, Supporting
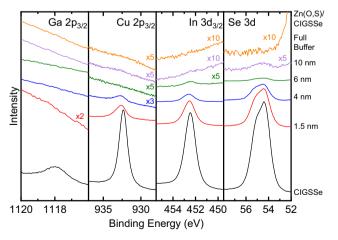
Information). Na is purposefully introduced in the process, beneficial for absorber growth, and known to be crucial for high solar cell efficiencies.[34–37] With increasing buffer layer thickness, the sodium intensity is significantly reduced but remains at a very low level for buffer layer thicknesses ≥ 4 nm. This suggests that sodium is either diffusing from the absorber onto the Zn(O,S) surface during the sputter-deposition process or, probably less likely, an impurity incorporated during the buffer layer growth.

To identify the chemical environment of zinc in the Zn(O,S) buffer layers, we compute the modified zinc Auger parameter α'_{Zn} by adding the binding energy of the Zn $2p_{3/2}$ peak and the kinetic energy of the Zn $L_3M_{45}M_{45}$ peak (Figure S3, Supporting Information). For the 1.5 nm Zn(O,S)/CIGSSe sample, we find a value of $\alpha'_{Zn} = 2010.79$ (± 0.07) eV, which increases slightly to 2010.85 (± 0.07) eV for the thickest buffer layer. A comparison with literature values (ZnO: 2009.90 eV $\leq \alpha'_{ZnO} \leq 2010.30$ eV; ZnS: 2011.3 eV $\leq \alpha'_{ZnS} \leq 2011.90$ eV)[23,38] indicates that Zn is neither in a pure oxide nor a pure sulfide environment.

To further investigate the Zn(O,S)/CIGSSe interface formation, the sample series was studied with XES. XES probes the local chemical environment from the perspective of an excited core level (here: S $2p$) and is a "photon-in photon-out" technique with significantly longer attenuation lengths as compared to the EAL above; for ZnS, for example, the attenuation lengths are 60 and 43 nm[39] for the incoming and outgoing photons, respectively. **Figure 4** shows the S $L_{2,3}$ emission spectra of the sample series. Note that the S $L_{2,3}$ emission overlaps with the Se $M_{2,3}$ emission, but the Se $M_{2,3}$ fluorescence yield is approximately two orders of magnitude lower than that of S $L_{2,3}$,[40] and thus its spectral contributions are negligible. The S $L_{2,3}$ spectra are normalized to the main peak (S $3s \rightarrow$ S $2p$ transition) at about 148 eV. The spectrum of the CIGSSe absorber (Figure 4, bottom spectra, black) is similar to already reported S $L_{2,3}$ Cu(In,Ga)(S,Se)$_2$ spectra.[2,18,41] The features in the region between 154–157 eV ("In $5s$-derived band" $\rightarrow$ S $2p$ transition)

Figure 3. Mg K_α XPS spectra of the Ga $2p_{3/2}$, Cu $2p_{3/2}$, In $3d_{3/2}$, and Se $3d$ peaks of the Zn(O,S)/CIGSSe interface as a function of increasing Zn(O,S) buffer layer thickness. Magnification factors are given on the right of the respective spectrum.

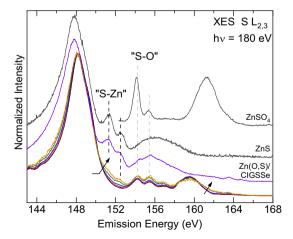**Figure 4.** S $L_{2,3}$ XES ($h\nu_{exc.} = 180$ eV) spectra of the CIGSSe absorber (black) and 1.5 (red), 4 (blue), 6 (green), 10 (orange), and fully buffered (purple) Zn(O,S)/CIGSSe. The latter, as well as the ZnS and ZnSO$_4$ reference spectra, are offset for better visibility. Black and gray dashed lines highlight signals that can be used as indicators for "S–Zn" and "S–O" bonds, respectively. Arrows illustrate the spectral evolution with increasing Zn(O,S) buffer layer thickness.

are indicative of S-In bonds. A broad feature at about 159 eV ("Cu 3d-derived band" → S 2p transition) highlights S-Cu bonds.[41,42] For increasing buffer layer thickness, additional intensity between 150–153 eV is detected and evolves into two additional peaks for a Zn(O,S) thickness at and above 6 nm (Figure 4, green). These peaks originate from transitions from electrons from Zn 3d-derived bands into the S 2p core holes and are characteristic for the presence of S–Zn bonds. This is most prominent for the thickest Zn(O,S)/CIGSSe sample. However, for this sample, the "dip" between the two peaks at ≈152 eV is not as deep as in the ZnS reference, which indicates a less well-defined chemical environment of the probed sulfur atoms. This is corroborated by two new weak signals at 154 and 155 eV, as well as a broader feature at ≈162 eV, which can be attributed to the formation of S-O bonds. For comparison, a ZnSO$_4$ reference spectrum is also shown to highlight the S–O bonding environment. Note that the chosen excitation energy of h$\nu_{exc.}$ = 180 eV is still resonant for sulfates and hence the spectral signature might change for small differences in excitation energy.[43] To avoid any artificial formation of S–O bonds due to the presence of sulfur and oxygen in the sample and the intense X-ray beam,[16] the samples were scanned under the X-ray beam. Hence, the observed spectral signature of the fully buffered Zn(O,S)/CIGSSe sample is a true "intrinsic feature", suggesting the presence of S–Zn and S–O bonds in the buffer layer. This is in agreement with the XPS S 2p core level spectrum of the thickest Zn(O,S)/CIGSSe spectrum, which also shows a weak sulfate signal even after ion treatment (Figure S4, Supporting Information).

As mentioned above, the O 1s XPS signal of all buffer layer samples consists of a hydroxide and an oxide component (Figure S1, Supporting Information). For the Zn(O,S) layers up to (including) 10 nm, the hydroxide component is larger than the oxide component; only for the fully buffered Zn(O,S)/CIGSSe sample, the situation is reversed. Here, we find a ZnO/(ZnO + Zn(OH)$_2$) area ratio of ≈60%. Other ZnO-related studies typically also find a hydroxide and an oxide component; in the case of a CBD-Zn(O,S) buffer layer, the hydroxide was significantly stronger than the oxide component.[9,13,44,45] Note that, after the Ar$^+$-ion treatment, the hydroxide component decreases ("dehydrogenation"). Similar effects are also reported for prolonged X-ray exposure and elevated temperatures.[9,13,44] In summary, thus, the analysis of the buffer layer suggests that a multitude of different bonding environments are presents, i.e., Zn–O, Zn–OH, Zn–S, and S–O bonds.

To investigate the electronic structure of the Zn(O,S)/CIGSSe interface, we have used a combination of UPS and IPES. With UPS and IPES, the relevant charge-carrier transport levels, i.e., the valence band maximum (VBM) and conduction band minimum (CBM), can be determined with a linear extrapolation of the leading edges in the spectra.[46,47] The UPS and IPES spectra of the 20 min Ar$^+$ ion-treated CIGSSe absorber and the as-received fully buffered Zn(O,S)/CIGSSe are shown in **Figure 5**. In case of the CIGSSe absorber, this surface treatment is necessary to remove surface adsorbates that would otherwise distort the spectral regions around the VBM and CBM. In case of the thick Zn(O,S)/CIGSSe sample, the influence of surface adsorbates is expected to be much less prominent and the hydroxides present at the surface (see discussion above and
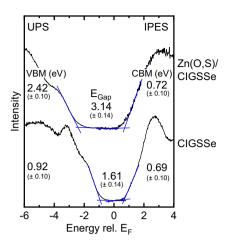

Figure 5. UPS and IPES spectra of the CIGSSe absorber and the fully buffered Zn(O,S)/CIGSSe sample. Energies are given relative to the Fermi energy. The determined valence band maximum (VBM) and conduction band minimum (CBM) values are given at the left and right of the graph, respectively. The resulting surface band gaps (E_{Gap}) are listed in the center. All values are given in eV.

Figure S1, Supporting Information) are very sensitive even to the mild 50 eV Ar$^+$ ion treatment. Thus, the as-received fully buffered Zn(O,S)/CIGSSe was chosen for the most reliable determination of VBM and CBM. For the absorber, we determine the VBM to 0.92 (±0.10) and the CBM to 0.69 (± 0.10) eV. These values suggest that the Fermi energy is above the "mid-gap" position at the absorber surface before interface formation. The sum of the VBM and CBM values gives a surface band gap of 1.61 (±0.14) eV. This value is significantly larger than the optically-derived minimal bulk band gap of 1.13 eV[20] and larger than the commonly found band gaps of high-efficiency copper-poor absorber surfaces[27] (≈1.4 eV) without sulfur and/or without Ga at the surface.[5,17,25,48,49] Here, we attribute the wider band gap to the fact that both S and Ga are found at the surface, both of which are expected to lead to a band-gap widening.[8,50]

For the thickest Zn(O,S)/CIGSSe sample, we find the VBM and CBM at 2.42 (±0.10) and 0.72 (±0.10) eV, respectively. For both the UPS and IPES spectra additional intensity is detected close to the VBM and CBM. Likely, these "tail states" can be related to defects, since their intensity is larger than would be expected based on the experimental resolution. For a different buffer layer (Zn,Mg)O, it was suggested that such tails are relevant for the charge carrier transport, while the spectral main edges are relevant for the optical properties.[51] Using the main edges, we derive a surface band gap of 3.14 (±0.14) eV, which is within the region of reported bulk Zn(O,S) band gap values of 2.6–3.4 eV, depending on the S/(S + O) ratio.[6,52,53]

The direct comparison of the band extrema allows a first approximation of the band alignment at the interface, suggesting no pronounced discontinuity in the conduction band and a significant negative valence band offset of ≈−1.5 eV. These values need to be corrected for the additional band bending induced by the interface formation.[54] To account for this, we used the 1.5 and 4 nm thin Zn(O,S)/CIGSSe samples, for which absorber-related lines were still visible in XPS. For the absorber, we

determined the relative shift using the In and Se $3d_{5/2}$ core levels. We did not use the Cu or Ga lines due to their low intensities. The band bending in the buffer layer was determined using the Zn $2p$, $3p$, $3d$, and O $1s$ core levels, as well as the Zn LMM Auger signal. The O $1s$ signal consists of an oxide (ZnO) and a hydroxide (ZnOH) component, as determined by fitting this region (Figure S1, Supporting Information). For the band-bending analysis, only the oxide values were used. Overall, we employed 24 different values to calculate the interface-induced band bending (Table S1, Supporting Information) and find an additional downward band bending in the absorber of -0.09 (± 0.03) eV. For the Zn(O,S) energy levels, we find an additional upward band bending of 0.10 (± 0.09) eV. As illustrated in **Figure 6**, we derive a flat conduction band alignment of 0.02 (± 0.16) eV and a valence band offset of -1.51 (± 0.16) eV, i.e., a significant hole barrier.

The derived flat conduction band alignment agrees with other experimentally derived flat conduction band alignments of high-efficiency thin-film solar cells.[10,25,48] Moreover, the additional small downward band bending in the absorber due to the interface formation (-0.09 (± 0.03)) will enhance the carrier separation at the interface. This is expected to be beneficial since it is accompanied by a lower recombination at the interface.

Comparing the results of the here-presented sputter-deposited Zn(O,S)/CIGSSe with the CBD-Zn(O,S)/CIGSSe interface,[9,10] we find some similarities and distinct differences. Both buffer layers consist of various bonding environments, e.g., sulfates and hydroxides, in addition to the expected mixture of Zn–O and Zn–S bonds. The CBD-Zn(O,S)/CIGSSe interface shows the diffusion of Se into the buffer layer while no diffusion of absorber elements into the sputtered Zn(O,S) layer is observed. Both band alignments (of high-efficiency devices) feature an essentially flat conduction band. However, the surface band gap of the CBD-Zn(O,S) is ≈ 0.4 eV smaller, likely due to a different S/(S + O) ratio and Se interdiffusion.
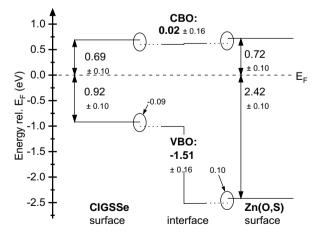

Figure 6. Schematic diagram of the band alignment at the Zn(O,S)/CIGSSe interface. The determined VBMs and CBMs of the CIGSSe and Zn(O,S) surfaces are shown on the left- and right-hand side, respectively. In the center, the derived conduction and valence band offsets of the Zn(O,S)/CIGSSe interface are shown. Changes due to the interface-induced band bending are indicated by ovals.

3. Summary

We have investigated a novel Cu(In,Ga)(S,Se)$_2$ absorber (a modified Avancis CIGSSe absorber, with Ga and S at the surface) and its interface with a sputter-deposited Zn(O,S) buffer layer by means of photoemission and Auger electron spectroscopy (sensitive to the surface) and X-ray emission spectroscopy (sensitive to the surface-near bulk). For the modified Avancis CIGSSe absorber, we find a surface band gap of 1.61 (± 0.14) eV. At the Zn(O,S)/CIGSSe interface, we find no indication for diffusion of absorber elements, Zn and S in a Zn(O,S) chemical environment, and the formation of some sulfate as well as hydroxide. Analyzing the electronic structure, we find an additional small downward band bending in the absorber due to the Zn(O,S)/CIGSSe interface formation, and derive a flat conduction band alignment at the Zn(O,S)/CIGSSe interface, as is compatible with high-efficiency chalcopyrite photovoltaic devices. In the future, the impact of alkali postdeposition treatments will be investigated, which pushes the conversion efficiencies of large-area cells with sputter-deposited Zn(O,S) buffer layer up to 19.8%.[22]

4. Experimental Section

The Cu(In,Ga)(S,Se)$_2$ absorbers were grown with a modified SEL-RTP (stacked elemental layer – rapid thermal processing) approach at the AVANCIS GmbH R&D center in Munich, Germany.[20] As we show in this paper, the absorber contains easily detectable amounts of Ga *and* S at the surface. Several Zn(O,S) buffer layers, with thicknesses ranging from ≈ 1.5 nm to the fully buffered sample (several tenths of nm), were directly sputter-deposited onto the CIGSSe absorbers. The thickness of each buffer layer was estimated based on the sputter time. To derive the electronic and chemical structure of the newly-engineered CIGSSe surface and its interface to sputter-deposited Zn(O,S), no additional alkali PDTs were performed. The Zn(O,S)/CIGSSe interface with a PDT step will be the topic of a future study.

The samples were shipped in a nitrogen-filled polyethylene bag to the University of Nevada, Las Vegas (UNLV) for XPS, UPS, and IPES measurements. At UNLV, the samples were directly inserted into an N$_2$-filled glovebox without any air exposure. In the glovebox, the samples were cut to produce three sets of samples. The first set was transferred directly into the ultrahigh vacuum multichamber system at UNLV (base pressure $\approx 1 \times$ E-10 mbar). All XPS data were collected with a Scienta R4000 electron analyzer and a SPECS XR 50 X-ray source. For the CIGSSe absorber, the UPS data was collected using a Gammadata VUV 5000 photon source and the Scienta R4000 electron analyzer, while the IPES data was measured with a STAIB low-energy electron source (NEK-150-1) and a Hamamatsu R6834 photomultiplier detector containing a band-pass entrance window (Semrock Hg01-254-25), detecting a fixed photon energy of 4.9 eV.[55] The UPS and IPES data of the fully buffered Zn(O,S)/CIGSSe sample were measured in a different apparatus, using a SPECS PHOIBOS 150 MCD electron analyzer and a He discharge lamp, as well as a STAIB low-energy electron source (NEK-150-1) and an I$_2$:Ar-filled photon detector, respectively.

After recording the "as-received" XPS, UPS, and IPES datasets, the adsorbates on the CIGSSe and Zn(O,S)/CIGSSe sample surfaces were reduced by a 50 eV Ar$^+$ ion treatment using a VG EX05 ion source for 20 and 10 min, respectively.

The second sample set was resealed under an inert atmosphere and shipped to the Materials for Energy (MFE) laboratory at the Karlsruhe Institute of Technology (KIT)[56] to also collect XPS data with Mg K_α and monochromatized Al K_α excitation for higher energy resolution. The surface characterization system of the MFE laboratory is equipped with Ar-filled gloveboxes, to allow for sample insertion without air

exposure, an Omicron Argus CU electron analyzer, a DAR450 twin anode X-ray source (Mg and Al K_α), and a monochromatized SIGMA Surface Science MECS X-ray source. At KIT, the samples were also Ar^+-ion treated after the initial measurements, for the same duration as at UNLV. The XPS data collected at UNLV and KIT agree very well—here, we present the XPS data collected at KIT (and the UPS and IPES data collected at UNLV). The energy scales of the electron spectrometers at UNLV and KIT were calibrated using the photoemission lines of sputter-cleaned copper, silver, and gold foils.[38,57] The Ag and Au foils were also used to calibrate the Fermi energy for UPS and IPES measurements.

The third sample set was also resealed under an inert atmosphere and shipped to Beamline 8.0.1 at the Advanced Light Source (ALS), Lawrence Berkeley National Lab, for soft X-ray emission spectroscopy (XES) measurements using our SALSA endstation and its high-transmission soft X-ray spectrometer.[58,59] During the XES measurements, the samples were continuously scanned under the soft X-ray beam with a speed of 30 μm s^{-1} to avoid any beam-induced changes. The S $L_{2,3}$ emission energy axis was calibrated using a CdS reference spectrum.[60]

Supporting Information

Supporting Information is available from the Wiley Online Library or from the author.

Acknowledgements

Conflict of Interest

The authors declare no conflict of interest.

Data Availability Statement

The data that support the findings of this study are available from the corresponding author upon reasonable request.

Keywords

[1] J. Palm, T. Dalibor, R. Lechner, S. Pohlner, R. Verma, R. Dietmüller, A. Heiß, H. Vogt, F. Karg, in *29th European Photovoltaic Solar Energy Conf. Exhibition*, Amsterdam, Netherlands **2014**, p. 1433.

[2] D. Hauschild, F. Meyer, A. Benkert, D. Kreikemeyer-Lorenzo, S. Pohlner, J. Palm, M. Blum, W. Yang, R. G. Wilks, M. Bär, C. Heske, L. Weinhardt, F. Reinert, *J. Phys. Chem. C* **2015**, *119*, 10412.

[3] M. Bär, N. Barreau, F. Couzinie-Devy, R. Felix, J. Klaer, S. Pookpanratana, M. Blum, Y. Zhang, J. D. Denlinger, W. Yang, R. G. Wilks, L. Weinhardt, H.-W. Schock, J. Kessler, C. Heske, in *Photovoltaic Specialists Conf. PVSC 2013 IEEE 39th*, IEEE, Piscataway, NJ **2013**, pp. 0857–0862.

[4] M. Bär, N. Barreau, F. Couzinié-Devy, L. Weinhardt, R. G. Wilks, J. Kessler, C. Heske, *ACS Appl. Mater. Interfaces* **2016**, *8*, 2120.

[5] D. Hauschild, F. Meyer, A. Benkert, D. Kreikemeyer-Lorenzo, T. Dalibor, J. Palm, M. Blum, W. Yang, R. G. Wilks, M. Bär, F. Reinert, C. Heske, L. Weinhardt, *Prog. Photovoltaics Res. Appl.* **2018**, *26*, 359.

[6] C. Persson, C. Platzer-Björkman, J. Malmström, T. Törndahl, M. Edoff, *Phys. Rev. Lett.* **2006**, *97*, 146403.

[7] M. Nakamura, K. Yamaguchi, Y. Kimoto, Y. Yasaki, T. Kato, H. Sugimoto, *IEEE J. Photovoltaics* **2019**, *9*, 1863.

[8] M. Bär, S. Nishiwaki, L. Weinhardt, S. Pookpanratana, O. Fuchs, M. Blum, W. Yang, J. D. Denlinger, W. N. Shafarman, C. Heske, *Appl. Phys. Lett.* **2008**, *93*, 244103.

[9] M. Mezher, R. Garris, L. M. Mansfield, M. Blum, D. Hauschild, K. Horsley, D. A. Duncan, W. Yang, M. Bär, L. Weinhardt, K. Ramanathan, C. Heske, *ACS Appl. Mater. Interfaces* **2016**, *8*, 33256.

[10] M. Mezher, R. Garris, L. M. Mansfield, K. Horsley, L. Weinhardt, D. A. Duncan, M. Blum, S. G. Rosenberg, M. Bär, K. Ramanathan, C. Heske, *Prog. Photovoltaics Res. Appl.* **2016**, *24*, 1142.

[11] L. Weinhardt, M. Bär, H.-J. Muffler, C.-H. Fischer, M. C. Lux-Steiner, T. P. Niesen, F. Karg, T. Gleim, C. Heske, E. Umbach, *Thin Solid Films* **2003**, *431–432*, 272.

[12] T. Adler, M. Botros, W. Witte, D. Hariskos, R. Menner, M. Powalla, A. Klein, *Phys. Status Solidi A* **2014**, *211*, 1972.

[13] M. Bär, A. Ennaoui, J. Klaer, T. Kropp, R. Sáez-Araoz, N. Allsop, I. Lauermann, H.-W. Schock, M. C. Lux-Steiner, *J. Appl. Phys.* **2006**, *99*, 123503.

[14] M. Bär, A. Ennaoui, J. Klaer, R. Sáez-Araoz, T. Kropp, L. Weinhardt, C. Heske, H.-W. Schock, C.-H. Fischer, M. C. Lux-Steiner, *Chem. Phys. Lett.* **2006**, *433*, 71.

[15] M. Sood, J. Bombsch, A. Lomuscio, S. Shukla, C. Hartmann, J. Frisch, W. Bremsteller, S. Ueda, R. G. Wilks, M. Bär, S. Siebentritt, *ACS Appl. Mater. Interfaces* **2022**, *14*, 9676.

[16] C. Heske, U. Groh, O. Fuchs, L. Weinhardt, E. Umbach, T. Schedel-Niedrig, C.-H. Fischer, M. C. Lux-Steiner, S. Zweigart, T. P. Niesen, F. Karg, J. D. Denlinger, B. Rude, C. Andrus, F. Powell, *J. Chem. Phys.* **2003**, *119*, 10467.

[17] L. Weinhardt, M. Morkel, T. Gleim, S. Zweigart, T. P. Niesen, F. Karg, C. Heske, E. Umbach, in *Proc. 17th EU PVSEC*, WIP-Renewable Energies, Munich, Germany **2001**, p. 1261.

[18] L. Weinhardt, O. Fuchs, A. Peter, E. Umbach, C. Heske, J. Reichardt, M. Bär, I. Lauermann, I. Kötschau, A. Grimm, S. Sokoll, M. C. Lux-Steiner, T. P. Niesen, S. Visbeck, F. Karg, *J. Chem. Phys.* **2006**, *124*, 074705.

[19] L. Weinhardt, M. Bär, S. Pookpanratana, M. Morkel, T. P. Niesen, F. Karg, K. Ramanathan, M. A. Contreras, R. Noufi, E. Umbach, C. Heske, *Appl. Phys. Lett.* **2010**, *96*, 182102.

[20] M. Stölzel, M. Algasinger, A. Zelenia, A. Weber, M. Sode, C. Schubbert, P. Eraerds, R. Lechner, T. Dalibor, J. Palm, in *Proc. 36th EU PVSEC*, WIP Renewable Energies, Marseille, France **2019**, pp. 590–596.

[21] M. Algasinger, T. Niesen, T. Dalibor, A. Steigert, R. Klenk, I. Lauermann, R. Schlatmann, M. C. Lux-Steiner, J. Palm, *Thin Solid Films* **2017**, *633*, 231.

[22] "New world record for CIGS efficiency," https://www.avancis.de/en/new-world-record-for-cigs-efficiency/ (accessed: November 2022).

[23] A. Naumkin, A. Kraut-Vass, S. Gaarenstroom, C. Powell, http://srdata.nist.gov/xps/Default.aspx (accessed: November 2022).

[24] J.-C. Dupin, D. Gonbeau, P. Vinatier, A. Levasseur, *Phys. Chem. Chem. Phys.* **2000**, *2*, 1319.

[25] D. Hauschild, D. Kreikemeyer-Lorenzo, P. Jackson, T. M. Friedlmeier, D. Hariskos, F. Reinert, M. Powalla, C. Heske, L. Weinhardt, *ACS Energy Lett.* **2017**, *2*, 2383.

[26] D. Kreikemeyer-Lorenzo, D. Hauschild, P. Jackson, T. M. Friedlmeier, D. Hariskos, M. Blum, W. Yang, F. Reinert, M. Powalla, C. Heske, L. Weinhardt, *ACS Appl. Mater. Interfaces* **2018**, *10*, 37602.

[27] D. Schmid, M. Ruckh, H. W. Schock, *Appl. Surf. Sci.* **1996**, *103*, 409.

[28] A. Kylner, *J. Electrochem. Soc.* **1999**, *146*, 1816.

[29] E. Handick, P. Reinhard, R. G. Wilks, F. Pianezzi, T. Kunze, D. Kreikemeyer-Lorenzo, L. Weinhardt, M. Blum, W. Yang, M. Gorgoi, E. Ikenaga, D. Gerlach, S. Ueda, Y. Yamashita, T. Chikyow, C. Heske, S. Buecheler, A. N. Tiwari, M. Bär, *ACS Appl. Mater. Interfaces* **2017**, *9*, 3581.

[30] S. Tougaard, http://www.quases.com/home/ (accessed: November 2022).

[31] S. Tanuma, C. J. Powell, D. R. Penn, *Surf. Interface Anal.* **1994**, *21*, 165.

[32] D. Hauschild, R. Steininger, D. Hariskos, W. Witte, S. Tougaard, C. Heske, L. Weinhardt, *J. Vac. Sci. Technol., A* **2021**, *39*, 063216.

[33] C. J. Powell, A. Jablonski, *Nucl. Instrum. Methods Phys. Res., Sect. A* **2009**, *601*, 54.

[34] C. Heske, G. Richter, Z. Chen, R. Fink, E. Umbach, W. Riedl, F. Karg, *J. Appl. Phys.* **1997**, *82*, 2411.

[35] C. Heske, D. Eich, R. Fink, E. Umbach, S. Kakar, T. van Buuren, C. Bostedt, L. J. Terminello, M. M. Grush, T. A. Callcott, F. J. Himpsel, D. L. Ederer, R. C. C. Perera, W. Riedl, F. Karg, *Appl. Phys. Lett.* **1999**, *75*, 2082.

[36] V. Probst, J. Rimmasch, W. Riedl, W. Stetter, J. Holz, H. Harms, F. Karg, H. W. Schock, in *IEEE Photovoltaic Specialists Conf. - 1994 IEEE First World Conf. Photovoltaic Energy Conversion. 1994 Conf. Record of the Twenty Fourth*, Vol. *1*, IEEE, Piscataway, NJ **1994**, pp. 144–147.

[37] M. Ruckh, D. Schmid, M. Kaiser, R. Schäffler, T. Walter, H. W. Schock, *Sol. Energy Mater. Sol. Cells* **1996**, *41–42*, 335.

[38] J. F. Moulder, W. F. Stickle, P. E. Sobol, K. D. Bomben, *Handbook of X-ray Photoelectron Spectroscopy*, Perkin-Elmer Corporation, Physical Electronics Division, Norwalk, Connecticut **1992**.

[39] E. M. Gullikson, http://henke.lbl.gov/optical_constants/ (accessed: November 2022).

[40] S. Pookpanratana, I. Repins, M. Bär, L. Weinhardt, Y. Zhang, R. Félix, M. Blum, W. Yang, C. Heske, *Appl. Phys. Lett.* **2010**, *97*, 074101.

[41] C. Heske, U. Groh, O. Fuchs, E. Umbach, N. Franco, C. Bostedt, L. J. Terminello, R. C. C. Perera, K. H. Hallmeier, A. Preobrajenski, R. Szargan, S. Zweigart, W. Riedl, F. Karg, *Phys. Status Solidi A* **2001**, *187*, 13.

[42] J. Reichardt, M. Bär, A. Grimm, I. Kötschau, I. Lauermann, S. Sokoll, M. C. Lux-Steiner, C.-H. Fischer, C. Heske, L. Weinhardt, O. Fuchs, C. Jung, W. Gudat, T. P. Niesen, F. Karg, *Appl. Phys. Lett.* **2005**, *86*, 172102.

[43] L. Weinhardt, D. Hauschild, R. Steininger, N. Jiang, M. Blum, W. Yang, C. Heske, *Anal. Chem.* **2021**, *93*, 8300.

[44] L. Weinhardt, C. Heske, E. Umbach, T. P. Niesen, S. Visbeck, F. Karg, *Appl. Phys. Lett.* **2004**, *84*, 3175.

[45] J. Duchoslav, R. Steinberger, M. Arndt, D. Stifter, *Corros. Sci.* **2014**, *82*, 356.

[46] T. Gleim, C. Heske, E. Umbach, C. Schumacher, S. Gundel, W. Faschinger, A. Fleszar, C. Ammon, M. Probst, H.-P. Steinrück, *Surf. Sci.* **2003**, *531*, 77.

[47] T. Gleim, C. Heske, E. Umbach, C. Schumacher, W. Faschinger, C. Ammon, M. Probst, H.-P. Steinrück, *Appl. Phys. Lett.* **2001**, *78*, 1867.

[48] M. Morkel, L. Weinhardt, B. Lohmüller, C. Heske, E. Umbach, W. Riedl, S. Zweigart, F. Karg, *Appl. Phys. Lett.* **2001**, *79*, 4482.

[49] D. Hauschild, E. Handick, S. Göhl-Gusenleitner, F. Meyer, H. Schwab, A. Benkert, S. Pohlner, J. Palm, S. Tougaard, C. Heske, L. Weinhardt, F. Reinert, *ACS Appl. Mater. Interfaces* **2016**, *8*, 21101.

[50] L. Weinhardt, O. Fuchs, D. Groß, G. Storch, E. Umbach, N. G. Dhere, A. A. Kadam, S. S. Kulkarni, C. Heske, *Appl. Phys. Lett.* **2005**, *86*, 062109.

[51] D. A. Duncan, R. Mendelsberg, M. Mezher, K. Horsley, S. G. Rosenberg, M. Blum, G. Xiong, L. Weinhardt, M. Gloeckler, C. Heske, *Adv. Mater. Interfaces* **2016**, *3*, 1600418.

[52] C. Platzer-Björkman, T. Törndahl, D. Abou-Ras, J. Malmström, J. Kessler, L. Stolt, *J. Appl. Phys.* **2006**, *100*, 044506.

[53] B. K. Meyer, A. Polity, B. Farangis, Y. He, D. Hasselkamp, Th Krämer, C. Wang, *Appl. Phys. Lett.* **2004**, *85*, 4929.

[54] E. A. Kraut, R. W. Grant, J. R. Waldrop, S. P. Kowalczyk, *Phys. Rev. Lett.* **1980**, *44*, 1620.

[55] H. Yoshida, *Chem. Phys. Lett.* **2012**, *539–540*, 180.

[56] L. Weinhardt, D. Hauschild, C. Heske, *Adv. Mater.* **2019**, *31*, 1806660.

[57] M. P. Seah, *Surf. Interface Anal.* **1989**, *14*, 488.

[58] M. Blum, L. Weinhardt, O. Fuchs, M. Bär, Y. Zhang, M. Weigand, S. Krause, S. Pookpanratana, T. Hofmann, W. Yang, J. D. Denlinger, E. Umbach, C. Heske, *Rev. Sci. Instrum.* **2009**, *80*, 123102.

[59] O. Fuchs, L. Weinhardt, M. Blum, M. Weigand, E. Umbach, M. Bär, C. Heske, J. Denlinger, Y.-D. Chuang, W. McKinney, Z. Hussain, E. Gullikson, M. Jones, P. Batson, B. Nelles, R. Follath, *Rev. Sci. Instrum.* **2009**, *80*, 063103.

[60] L. Weinhardt, O. Fuchs, A. Fleszar, M. Bär, M. Blum, M. Weigand, J. D. Denlinger, W. Yang, W. Hanke, E. Umbach, C. Heske, *Phys. Rev. B* **2009**, *79*, 165305.

2201091 (7 of 7)